Research Paper

Application of Double Q Wavelet-based Sparse Decomposition to Fault Feature Extraction of Wind Turbine Planetary Gearbox

Jin XU[1,2)], Xian DING[1,2)]*, Zhu ZHANG[3)], Lang CHEN[3)]

[1)] *China Green Development Investment Group CO. LTD.*
Beijing 100020, China

[2)] *Luneng Group CO. LTD.*
Beijing, 100020, China
*Corresponding Author e-mail: fd_dingxian@163.com

[3)] *Jiangsu Goldwind Science & Technology CO. LTD.*
Yancheng, 224100, China

The wind turbine gearbox is a critical equipment transforming the speed of the rotor hub to the generator, the condition of which is the reflection of operational efficiency and reliability of wind turbines. As the initial stage of the wind turbine gearbox, the fault feature extraction of the planetary gear set is challenging since it is prone to be affected by complicated structure, vibration from other high-speed stages and background noise. In this paper, a double Q factor wavelet-based sparse decomposition is applied to the fault feature extraction of the wind turbine planetary gearbox. Considering the sparsest wavelet coefficients, the vibration signal is iteratively decomposed into high Q and low Q components. The fault feature is generally hidden in the low Q component. With further demodulation, the fault information of planetary gears can be easily detected.

Key words: wind turbine gearbox; planetary gears; double Q factor wavelet; sparse decomposition.

1. Introduction

Wind energy is an important pillar of renewable energy, which has developed rapidly in recent years. By the end of 2020, China's installed wind power capacity has reached 280 million kW [1], accounting for 5.5% of the electricity supply. As the conversion carrier of wind energy to electric energy, wind turbines operate under alternating load, extreme temperature difference and other harsh operating conditions for long periods of time, and their failure rate is high. As wind turbines usually operate at high altitudes, the maintenance tasks for subassemblies are exceptionally challenging, leading to long downtime and high maintenance costs.

Horizontal-shaft wind turbine with speed-increasing gearbox is the prevailing type of wind power generation, accounting for about 80% of the total installed capacity [2]. The wind turbine gearbox is responsible for converting the impeller's low speed into the generator's high speed. To achieve a large transmission ratio in limited space, the wind turbine gearbox is usually composed of a planetary stage gear set and a parallel stage gear set. The planetary stage gear set is located at the low-speed end, namely the power input end, where the load is heavier than at the high-speed end. Since the ring gear encloses the planet gears, sun gear and planet bearings, it is difficult for any metal fragments from faulty planetary stage gears to fall into the bottom of the shell but they can easily be embedded in the planetary stage gear clearance. This phenomenon will inevitably cause the planetary transmission to jam, and even the whole gearbox body to burst. In a nutshell, the consequences brought by the faulty planetary transmission are more serious than those from the parallel gear transmission.

The fault feature extraction and diagnosis for planetary gears have attracted considerable attention. FENG and ZUO [3] proposed the vibration model of planetary gears under fault states and presented the calculation method of fault characteristic frequency of planet gear, sun gear and ring gear. Based on this, the iterative generalized synchro squeezing transform [4] and the adaptive optimal kernel time-frequency analysis [5] were proposed to extract fault features of planetary gears under non-stationary conditions. LEI *et al.* [6] used the adaptive stochastic resonance method to realize fault diagnostics of the planetary gear. ZHANG *et al.* [7] integrated the Teager energy operator (TEO) demodulation and stochastic resonance method to detect early faults of the planetary gearbox. LIANG *et al.* [8] proposed a vibration signal model of a planetary gear set considering the effect of multiple vibration sources and changing transmission path.

The above research provided important findings for the fault feature extraction and diagnosis methods for planetary gears but mainly focused on the pure planetary gear transmission with a relatively simple structure. Several challenges exist in fault feature extraction of planetary gears in the wind turbine gearbox with multistage transmissions:

1) The rotational speed of planetary gears is relatively low. Correspondingly, the fault features of the planetary gears will be weak and can be easily concealed by the meshing energy of the parallel stage gears or background noise.

2) There are multiple gears and bearings in the wind turbine gearbox. The low fault characteristic frequencies of the components in the planetary gear set are close to each other, so that the discrimination degree is insufficient, which may cause an incorrect identification of problem.

Wavelet-based sparse decomposition methods have proven effective in fault diagnosis of rotating machineries, e.g., gears, bearings, etc. Under the resonance-based signal decomposition framework with the L1 norm regularization [9] and tunable Q wavelet transform (TQWT) [10], CAI *et al.* [11] employed the morphological component analysis to estimate and separate different resonance components of gearbox vibration signal, and solved the optimization problem by the split augmented Lagrangian shrinkage algorithm. DU *et al.* [12] proposed a sparse framework considering noise to decompose the vibration signal from the wind turbine gearbox and successfully detected the weak gear fault characteristics. To overcome the potential underestimation of the signal component of L1 norm, a series of non-convex penalty functions, e.g., atan, log, rat, etc., were combined in signal sparse representation, and have been applied in the multi-faults detection of milling stand gearbox [13] and planetary subassemblies in wind turbine gearbox [14]. A multivariate generalization of the minimax-concave (MC) penalty was proposed by SELESNICK [15] in sparse approximate solutions. Afterward, CAI *et al.* [16] and WANG *et al.* [17] developed MC penalty-based sparse methods to detect gearbox faults. Although the L1 norm often underestimates the true solution, there are still advantages in the L1 norm sparse decomposition compared to other non-convex penalty functions:

1) The optimization problem using the L1 norm can guarantee the convex and global optimal solution with fast computation.

2) The L1 algorithm avoids several sub-problems when solving non-convex penalty-based sparse decomposition, which reduces the method complexity.

Based on the analysis aforementioned, the double Q wavelet-based sparse decomposition with the L1 norm, an existing signal processing technique, is used in this paper to analyze the vibration signal collected from the on-site gearbox to accurately detect the fault features of planetary gears in wind turbine gearbox. TQWT enables to decompose vibration signals as their resonance characteristic with different quality factors. Further, under the sparse decomposition framework, the vibration signal is expressed by more concise wavelet atoms to accurately extract the intrinsic features. The vibration signal is iteratively decomposed into low Q and high Q components, in which the low Q component matches the impact process caused by potential faults, while the high Q component represents the normal meshing and noise information of the faultless gears. Through the envelope demodulation analysis for the decomposed low Q component, weak planet gear faults covered by complex information can be found distinctly. The double Q wavelet-based sparse decomposition provides an effective tool for detecting incipient planet gear faults of the wind turbine gearbox, which can assist in avoiding catastrophic results at the wind farm.

2. Tunable Q wavelet transform

In the wavelet transform, the quality factor Q is defined as the ratio of the wavelet bandwidth to the center frequency. Generally, the wavelet transform has the characteristic of constant Q. SELESNICK [10] proposed a wavelet transform (tunable Q wavelet) that can adjust the Q factor arbitrarily. Wavelets with different Q factors have different oscillation properties, which can match various vibration components during the operation of mechanical components [11].

The decomposition and reconstruction process of tunable Q wavelet transform is shown in Fig. 1, which is similar to the conventional wavelet transform.
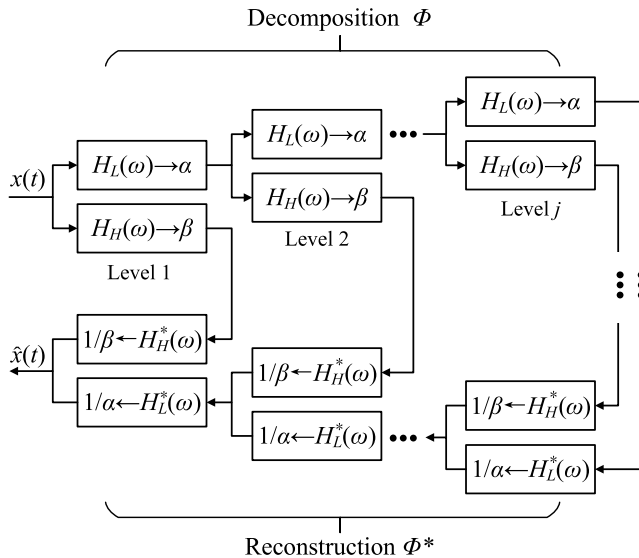

FIG. 1. The decomposition and reconstruction process of tunable Q wavelet transform.

Like the conventional dyadic wavelet transform, tunable Q wavelet transform gradually decomposes the signal from high to low frequency. Merely the quality factor can be set artificially to adapt different signal resonance characteristics. The difference is that the tunable Q wavelet introduces low-pass scale factor α and high-pass scale factor β, and the relationship between α, β and quality factor Q can be described as

$$(2.1) \qquad \beta = \frac{2}{Q+1},$$

$$(2.2) \qquad \alpha = 1 - \frac{\beta}{r} = 1 - \frac{2}{r(Q+1)}.$$

In Eq. (3.2), r is the redundancy denoting the oversampled degree $r = \beta/(1-\alpha)$. Based on the above parameters, the maximum decomposition level of tunable Q wavelet is calculated as

$$(2.3) \qquad J_{\max} = \left\lfloor \frac{\log(\beta N/8)}{\log(1/\alpha)} \right\rfloor,$$

where $\lfloor \ \rfloor$ means negative rounding operation, N is the signal length. For the j-th decomposition, the equivalent frequency response function of the wavelet filter is

$$(2.4) \quad H_L^{(j)}(\omega) = \begin{cases} \displaystyle\prod_{i=0}^{j-1} H_L\left(\frac{\omega}{\alpha^i}\right), & |\omega| \le \alpha^j \pi, \\ 0, & \text{other}, \end{cases}$$

$$(2.5) \quad H_H^{(j)}(\omega) = \begin{cases} \displaystyle H_H\left(\frac{\omega}{\alpha^{j-1}}\right)\prod_{i=0}^{j-2} H_L\left(\frac{\omega}{\alpha^i}\right), & (1-\beta)\alpha^{j-1}\pi \le |\omega| \le \alpha^{j-1}\pi, \\ 0, & \text{other}, \end{cases}$$

where $H_L(\omega)$ is the frequency response of the low-pass filter, $H_H(\omega)$ is the frequency response of the high-pass filter, and their expressions are

$$\begin{cases} |H_L(\omega)| = 1, & |\omega| \le (1-\beta)\pi, \\ H_L(\omega) = 0, & \alpha\pi \le |\omega| \le \pi, \end{cases}$$

$$\begin{cases} |H_H(\omega)| = 0, & |\omega| \le (1-\beta)\pi, \\ H_H(\omega) = 1, & \alpha\pi \le |\omega| \le \pi. \end{cases}$$

The transition bands of $H_L(\omega)$ and $H_H(\omega)$ must be chosen as

$$|H_L(\omega)|^2 + |H_H(\omega)|^2 = 1.$$

Primarily, they can be designed as the Daubechies frequency response

$$(2.6) \qquad H_L(\omega) = \theta\left(\frac{\omega + (\beta-1)\pi}{\alpha + \beta - 1}\right),$$

$$(2.7) \qquad H_H(\omega) = \theta\left(\frac{\alpha\pi - \omega}{\alpha + \beta - 1}\right).$$

The above filter banks are designed by the Daubechies frequency response with two-order vanishing moments [18]

$$(2.8) \qquad \theta(\omega) = 0.5(1 + \cos\omega)\sqrt{2 - \cos\omega}, \qquad |\omega| \le \pi.$$

3. DOUBLE Q WAVELET-BASED SPARSE DECOMPOSITION

In morphological analysis, it is assumed that the original signal x is composed of two types of signals with different vibration properties, and the background noise n

$$(3.1) \qquad\qquad x = x_1 + x_2 + n,$$

where x_1 is the high Q component in the signal, which usually represents the smooth component of normal gear meshing in rotating machinery, and x_2 is the low Q component in the signal, which represents the impact component caused by potential fault. If x_1 and x_2 are separated from x, the fault components hidden in the signal will be more distinctly revealed. The sparse decomposition method aims at the sparsest wavelet coefficients of all levels of components under different tunable Q wavelet decomposition [9]:

$$(3.2) \qquad \begin{aligned} \{\omega_1^{\mathrm{opt}}, \omega_2^{\mathrm{opt}}\} &= \arg\min_{\omega_1,\omega_2} \|\omega_1\|_1 + \|\omega_2\|_1\,, \\ \text{s.t.} \quad &\|x - \Phi_1^* \omega_1 - \Phi_2^* \omega_2\|_2 \le \varepsilon, \end{aligned}$$

where ω_1 and ω_2 are wavelet coefficients after high Q and low Q wavelet transform, Φ_1^* and Φ_2^* indicate the inverse transform of tunable Q wavelet, representing the reconstruction process from wavelet coefficients to vibration signal, and ε is the limited noise. The L1 norm is used to evaluate the sparsity of the wavelet coefficients.

Converting Eq. (3.2) into an unconstrained problem, the optimal problem is expressed as

$$(3.3) \qquad \{\omega_1^{\mathrm{opt}}, \omega_2^{\mathrm{opt}}\} = \arg\min_{\omega_1,\omega_2} \|x - \Phi_1^* \omega_1 - \Phi_2^* \omega_2\|_2^2 + \lambda_1 \|\omega_1\|_1 + \lambda_2 \|\omega_2\|_1\,,$$

where λ_1 and λ_2 are the Lagrange multipliers. They can be further denoted by

$$\lambda_1 = \theta_1 \|\psi_1\|_2\,, \qquad \lambda_2 = \theta_2 \|\psi_2\|_2\,,$$

where ψ_1 and ψ_2 are the wavelet corresponding to the wavelet coefficients ω_1 and ω_2 in high Q and low Q wavelet transform. The scalar parameters θ_1 and θ_2 are associated with the signal and the estimation error, which are used to adjust the relative energy of the high Q and low Q components.

Since the L1 norm is not differentiable, the split augmented Lagrange shrinkage algorithm [19] is adopted to solve the above unconstrained problem, which is defined as

$$\begin{aligned} f_1(\mathbf{u}) &= \|x - \Phi_1^* u_1 - \Phi_2^* u_2\|_2^2\,, \\ f_2(\omega) &= \lambda_1 \|\omega_1\|_1 + \lambda_2 \|\omega_2\|_1\,, \end{aligned}$$

where $\mathbf{u} = [u_1, u_2]$ is a temporary variable. Equation (3.3) is solved by alternating split-augmented Lagrange algorithm, which can be expressed as

$$(3.4) \qquad \mathbf{u}^{(k+1)} = \arg\min_{\mathbf{u}} \; \|x - \Phi_1^* u_1 - \Phi_2^* u_2\|_2^2 + \mu \left\|\mathbf{u} - \boldsymbol{\omega}^{(k)} - \mathbf{d}^{(k)}\right\|_2^2,$$

$$(3.5) \qquad \boldsymbol{\omega}^{(k+1)} = \arg\min_{\boldsymbol{\omega}} \lambda_1 \|\omega_1\|_1 + \lambda_2 \|\omega_2\|_1 + \mu \left\|\mathbf{u}^{(k+1)} - \boldsymbol{\omega} - \mathbf{d}^{(k)}\right\|_2^2,$$

$$(3.6) \qquad \mathbf{d}^{(k+1)} = \mathbf{d}^{(k)} - \mathbf{u}^{(k+1)} + \boldsymbol{\omega}^{(k+1)},$$

where μ is the introduced penalty parameter. After multiple iterations, the optimal wavelet coefficients ω_1^{opt} and ω_2^{opt} of high Q and low Q components with sparsity can be obtained. Further, the high Q and low Q components will be constructed by the wavelet coefficients.

4. Case study

4.1. Testing condition of the wind turbine

The tested wind turbine is a 1.5 MW doubly-fed unit, whose gearbox structure incorporates two-stage planetary gear sets combined with one-stage parallel gear transmission, shown in Fig. 2. Wind energy absorbed by the blades is converted into the rotating mechanical energy of the rotor hub, which is further accelerated by the speed-increasing gearbox and converted into the high-speed mechanical energy that drives the rotation of the generator.
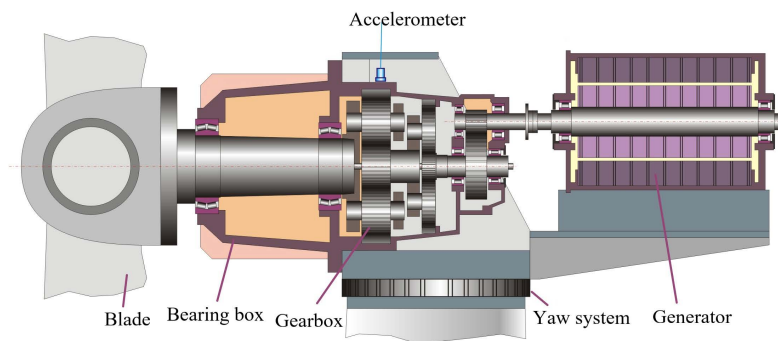

Fig. 2. Structure of the wind turbine gearbox.

The number of teeth of all stages of gears in the speed-increasing gearbox are shown in Table 1. When the rotational speed of the rotor hub is 18 r/min (0.3 Hz), the rotational frequencies of each shaft in the gearbox are shown in Table 2 where f_{c1} is the rotational frequency of the rotor hub, namely the carrier of the first PS, f_{s1} is the rotational frequency of the sun gear in the

Table 1. The number of teeth of multiple gears in the wind turbine gearbox.

Nomenclature	Number	Description
Z_{p1}	34	number of teeth of the planet gear in the first planetary stage (PS)
Z_{s1}	23	number of teeth of the sun gear in the first PS
Z_{r1}	91	number of teeth of the ring gear in the first PS
Z_{p2}	45	number of teeth of the planet gear in the second PS
Z_{s2}	25	number of teeth of the sun gear in the second PS
Z_{r2}	116	number of teeth of the ring gear in the second PS
Z_{hi}	101	number of teeth of the input gear in the high-speed parallel stage
Z_{ho}	28	number of teeth of the output gear in the high-speed parallel stage

Table 2. Shaft rotating frequencies and gear meshing frequencies.

Nomenclature	Number	Description
f_{c1}	0.3	rotating frequency of the rotor hub (rotating frequency of the carrier of the first PS)
f_{s1} (f_{c2})	1.42	rotating frequency of the sun gear in the first PS (rotating frequency of the carrier of the second PS)
f_{s2}	8.04	rotating frequency of the sun gear in the second PS (rotating frequency of the input gear in the high-speed parallel stage)
f_h	29	rotating frequency of the output gear in the high-speed parallel stage
f_{PS1}	26.2	meshing frequency of the first PS
f_{PS2}	165.3	meshing frequency of the second PS
f_{HSS}	812	meshing frequency of the high-speed parallel stage

first PS, equivalent to the frequency f_{c2} of the carrier of the second PS, f_{s2} is the rotational frequency of the sun gear in the second PS, f_h is the rotational frequency of the output shaft of the wind turbine gearbox, and f_{PS1}, f_{PS2} and f_{HSS} are respectively the meshing frequencies of the first PS, the second PS and the parallel gears. The meshing frequencies of the three stages in the wind turbine gearbox are calculated as follows:

- the first PS $f_{\mathrm{PS1}} = f_{c1} \cdot Z_{r1} = (f_{c2} - f_{c1})Z_{s1}$,
- the second PS $f_{\mathrm{PS2}} = f_{c2} \cdot Z_{r2} = (f_{s2} - f_{c2})Z_{s2}$,
- the high-speed stage $f_{\mathrm{HSS}} = f_{s2}Z_{hi} = f_h Z_{ho}$.

The shaft rotating frequencies are shown as:

- the sun shaft of the first PS (the planet carrier of the second PS) $f_{c2} = f_{c1}(1 + Z_{r1}/Z_{s1})$,
- the sun shaft of the second PS $f_{s2} = f_{c2}(1 + Z_{r2}/Z_{s2})$,
- the high-speed shaft $f_h = f_{s2} \cdot Z_{hi}/Z_{ho}$.

The fault characteristic frequency of planet gear in the first PS is calculated as $2f_{c1}Z_{r1}/Z_{p1}$, the characteristic frequency of ring gear in the first PS is $3f_{c1}$, and the characteristic frequency of sun gear in the first PS is $3(f_{c2} - f_{c1})$. Similarly, the fault characteristic frequency of planet gear in the second PS is calculated as $2f_{c2}Z_{r2}/Z_{p2}$, the characteristic frequency of ring gear in the second PS is $3f_{c2}$, and the characteristic frequency of sun gear in the first PS is $3(f_{s2} - f_{c2})$. The characteristic frequencies of input and output gears in the high-speed stage are separately f_{s2} and f_h.

When the rotational speed of the rotor hub is 18 r/min (0.3 Hz), the fault characteristic frequency of planet gear in the first PS $2 \times f_{c1} \times Z_{r1}/Z_{p1} = 2 \times 0.3 \times 91/34 = 1.6$ Hz. In Fig. 2, the accelerometer is installed on the surface of the wind turbine gearbox to monitor the condition of the planetary subassemblies. The vibration data from the accelerometer (shown in Fig. 2) collected within nine days are shown in Fig. 3a. The data was collected every half an hour, and 48 groups were collected each day. There are 414 groups of vibration signals in Fig. 3a. Since the planetary gear set is located at the input end of the gearbox, with lower rotational speed, the sampling frequency is set as 2560 Hz and the sampling duration is 6.4 s. Figures 3b and 3c are respectively the root mean square (RMS) and kurtosis corresponding to the long time signal. As shown
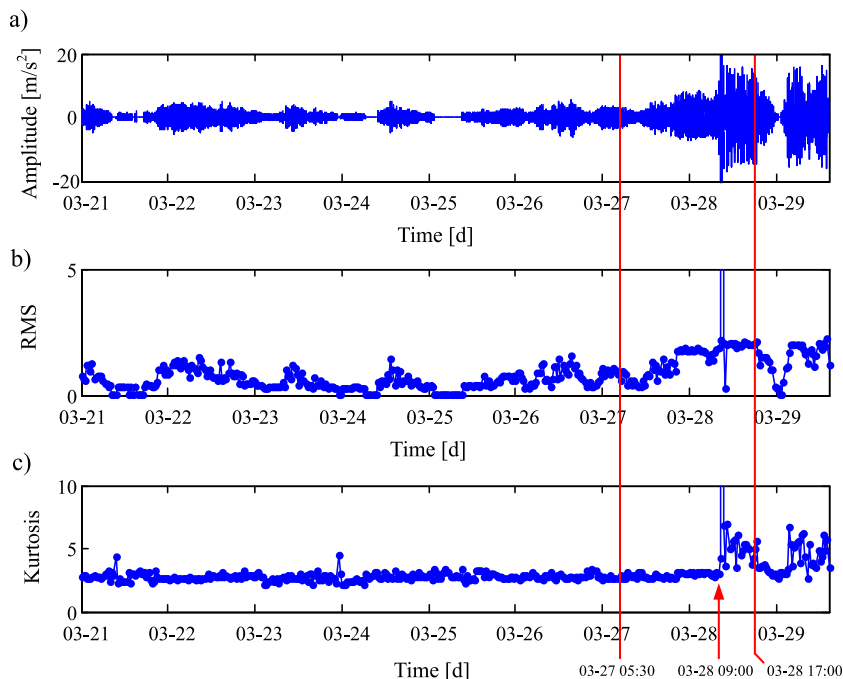

FIG. 3. Long-term vibration signal and the features:
a) temporal signal, b) root mean square, c) kurtosis.

in Fig. 3, starting from 9:00 on March 28, the signal's amplitude increased significantly, and the RMS and kurtosis exhibited an abrupt change as well, denoting that the overall state of the first planetary stage gears deteriorated at this time. After that, the signal's vibration amplitude, RMS and kurtosis always remained at high level, indicating that the monitored subassemblies had irreversible failures.

Generally, weak faults emerge before the mechanical parts fail, but the fault symptoms are weak, concealed by the background noise or other vibration sources. As shown in Fig. 3a, the vibration amplitude before 9:00 on March 28 is low, and it is difficult to obtain effective fault symptoms from the original vibration signals. For this reason, the double Q wavelet sparse decomposition method is used to analyze the vibration signal at 5:30 on March 27, and the vibration signal at this time is shown in Fig. 4a.
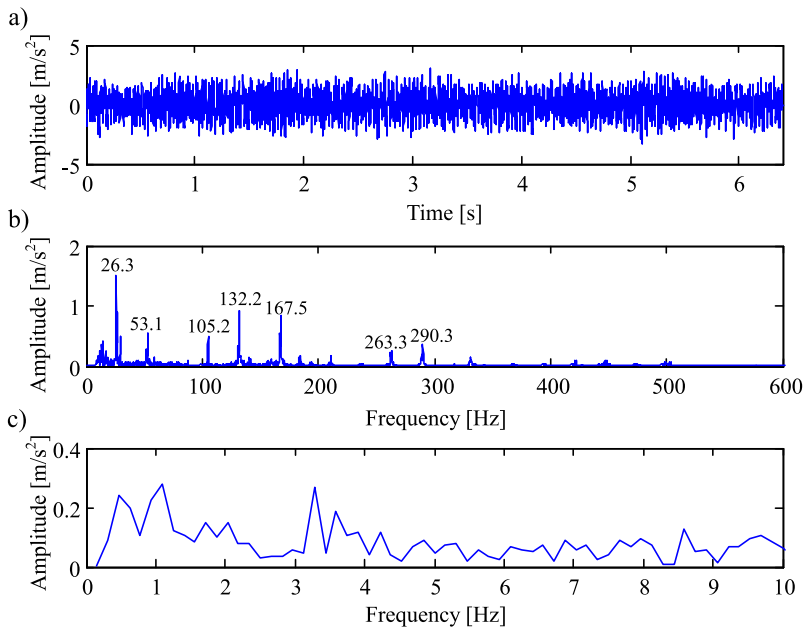
FIG. 4. Vibration signal: a) vibration signal, b) frequency spectrum, c) envelope spectrum.

In Fig. 4a, the vibration amplitude is relatively stable, and no evident fault features can be found from the time signal. The frequency spectrum at 5:30 on March 27 is shown in Fig. 4b. Frequency components such as 26.3 Hz, 53.1 Hz, 105.2 Hz and 132.2 Hz are distinct in the figure, corresponding to the first-, second-, fourth-, and fifth-order meshing frequencies of the first planetary gear set. In addition, there is also a prominent component of 167.5 Hz, which is the meshing frequency of the second planetary gear set. The occurrence of the

above meshing frequencies belongs to the normal meshing vibration of the wind turbine gearbox. Figure 4c is the envelope spectrum of the vibration signal, where there is no obvious impact component in the figure.

4.2. Fault extraction using double Q wavelet-based sparse decomposition

Double Q wavelet-based sparse decomposition is performed for the vibration signals at 5:30 on March 27, where the high Q factor $Q_1 = 16$, the wavelet redundancy $r_1 = 12$, and the relevant parameters of the low Q wavelet are $Q_2 = 1$ and $r_2 = 8$. As expressed above, the scalar parameters θ_1 and θ_2 are associated with the signal and the estimation error, which are used to adjust the relative energy of the high Q and low Q components. Referring to the fact that the similar θ_1 and θ_2 can generate superior decomposed results [11, 14], we set $\theta_1 = \theta_2 = 2$. The decomposed high Q component is shown in Fig. 5b, and the
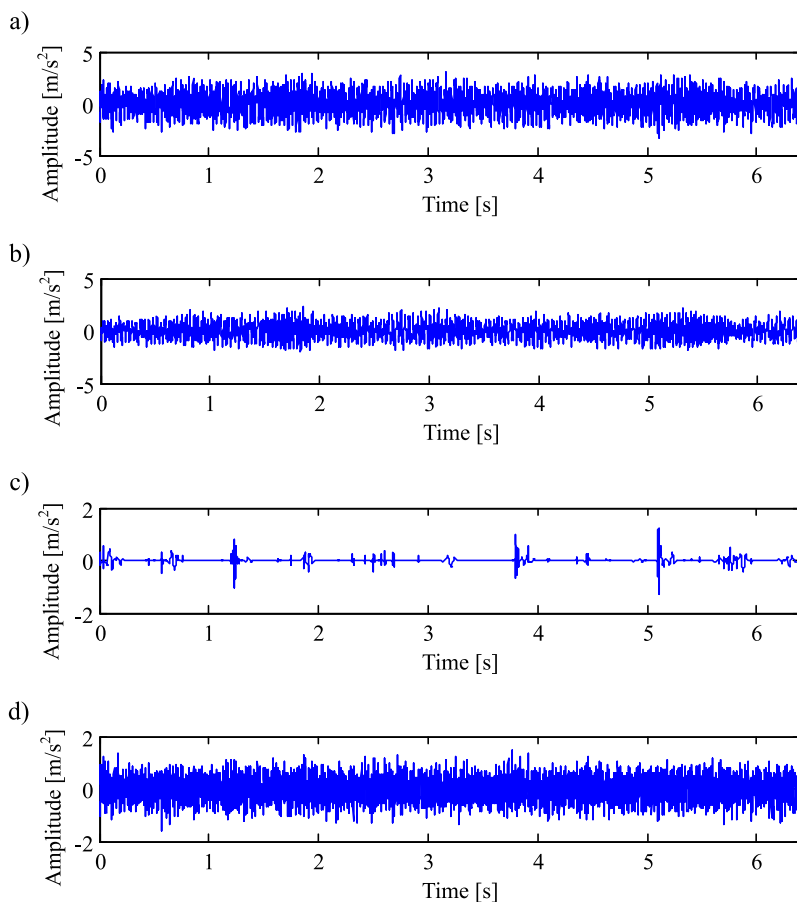

FIG. 5. Vibration signal and the decomposed results: a) vibration signal, b) high Q component, c) low Q component, d) noise.

decomposed low Q component is shown in Fig. 5c. Noise is shown in Fig. 5d. There is an obvious impact process in the low Q component. The envelope signal of the low Q component is shown in Fig. 6a, and its envelope spectrum is shown in Fig. 6b. A clear 1.72 Hz appears in Fig. 6b, which is consistent with the calculated planet gear fault characteristic frequency (1.6 Hz). It can be inferred that the planet gear was in an faulty state at this time. However, the corresponding fault characteristics cannot be detected by the conventional analysis in Fig. 4. By contrast, the periodic fault impact of the planet gear is successfully found in the low Q component through the double Q wavelet-based sparse decomposition.
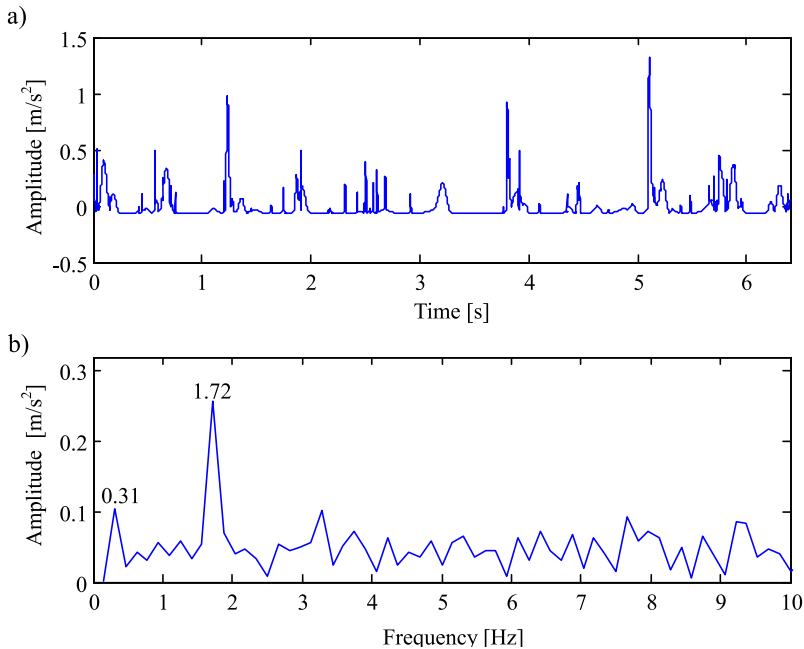
FIG. 6. Low Q component and its envelope: a) envelope of the low Q component, b) envelope spectrum of the low Q component.

After the notable failure of the planet gear at 9:00 on March 28, the vibration signal at 17:00 on March 28 is shown in Fig. 7a. There is a regular impact process in the signal, but it is greatly affected by high- frequency signals and noises. Vibration signals are decomposed using the same double Q wavelet sparse decomposition method, and the decomposed high Q component is shown in Fig. 7b, which is dominated by high-frequency meshing vibrations. The low Q component after decomposition is shown in Fig. 7c, where distinct impact vibrations appear, indicating that the proposed method can effectively separate the impact components from original signals.
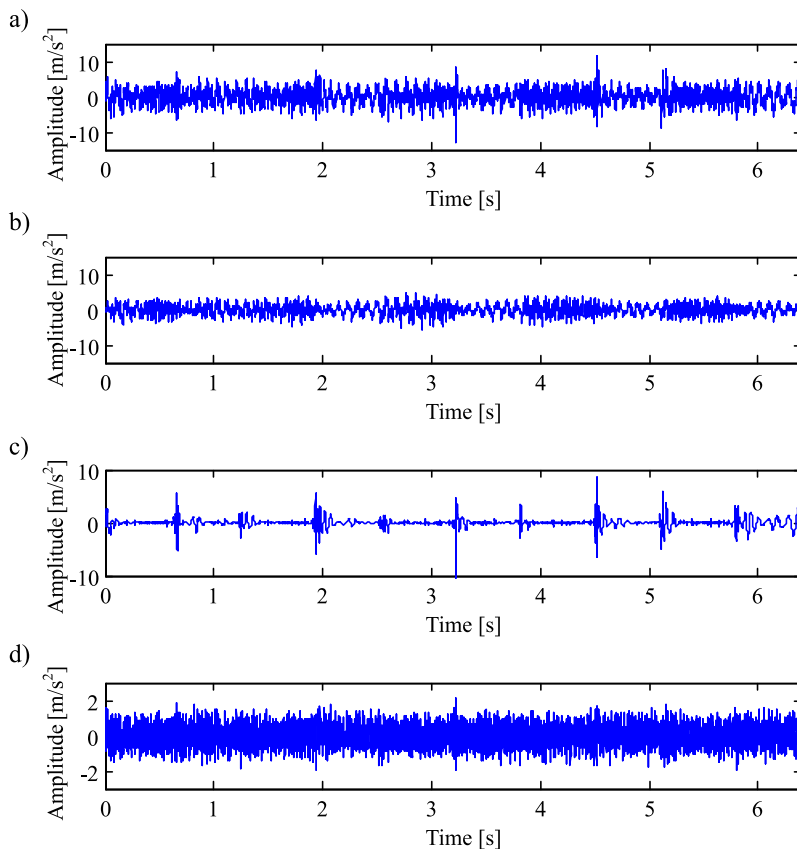
FIG. 7. Vibration signal and the decomposed results: a) vibration signal, b) high Q component, c) low Q component, d) noise.

The envelope signal of the isolated low Q component is shown in Fig. 8a. The envelope spectrum of the envelope signal is calculated and shown in Fig. 8b. In the latter figure, 1.72 Hz and 3.3 Hz are clearly presented, corresponding to the planet gear's first-order and second-order fault characteristic frequencies in the first planetary stage gear set in the wind power gearbox. The above analysis once again demonstrates the effectiveness of the double Q-based sparse decomposition in extracting the fault characteristic frequency of the planet gears. Figures 5 and 6 show that the proposed method is valid even though the fault is in the incipient phase.

To study the fault tendency during the eight days, 414 groups of vibration signals are decomposed by the double Q wavelet-based sparse method with identical parameters. The envelope spectrum of the low Q components that represent potential faults is shown in Fig. 9. We can see that the weak fault characteristic exists before March 28, and the demodulated vibration amplitude increases
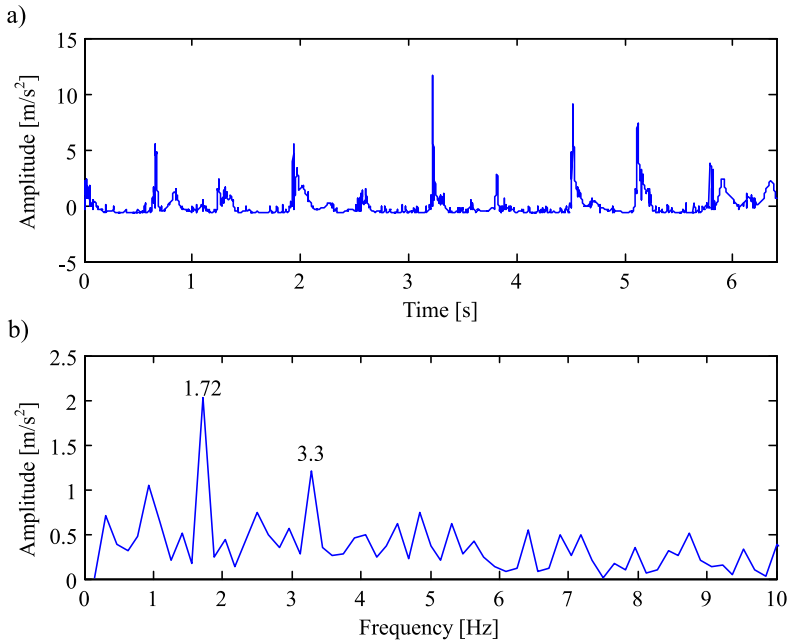
a)

b)

FIG. 8. Low Q component and its envelope: a) envelope of the low Q component, b) envelope spectrum of the low Q component.
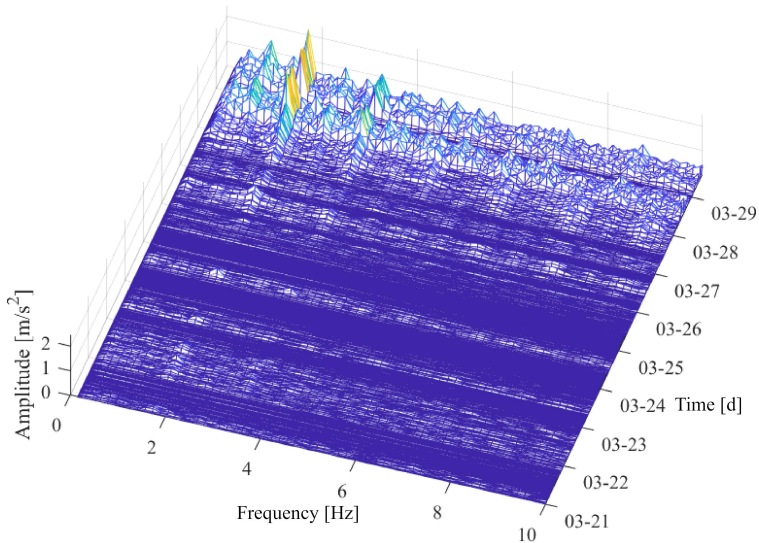

FIG. 9. The 3-D envelope spectrum of the low Q components of 414 groups of vibration signals.

gradually with the fault deterioration. The fault characteristic is 1.72 Hz, corresponding to the fault of planet gears.

Figure 10 shows the root crack of the planet gear in the first planetary stage gear set, which was observed through the peephole. The picture verifies the analysis result above.

FIG. 10. Root flaw of the planet gear.

4.3. Comparison analysis

Without considering the sparsity of wavelet coefficient, only the low Q wavelet transform is used to analyze the vibration signal collected from 5:30 on March 27. $Q_2 = 1$ and $r_2 = 8$. After the TQWT transform, the wavelet coefficients are reconstructed at different frequency bands, *i.e.*, the different decomposition stages. The envelope spectrum of the reconstructed signal at different stages is shown in Fig. 11. The fault characteristic frequency of planet gears (1.7 Hz) cannot be found, and only 3.28 Hz (approximating the twice of 1.7 Hz) is distinct. The
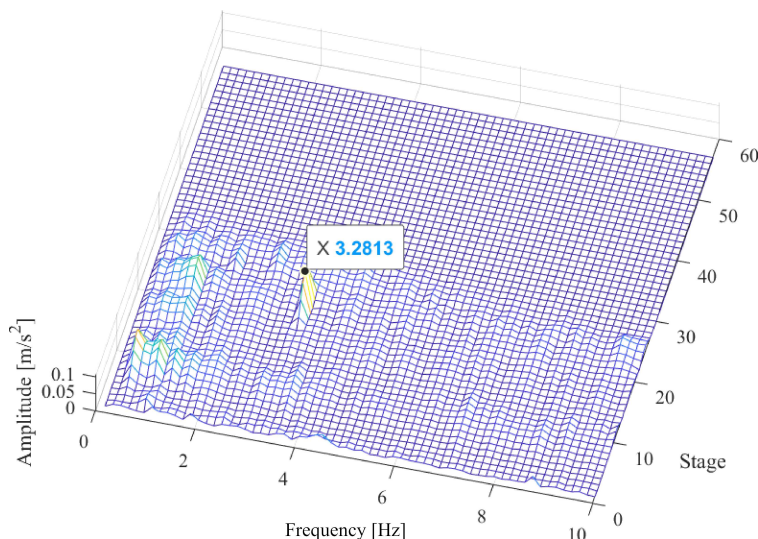

FIG. 11. The envelope spectrum of the reconstructed signal only using a low Q wavelet transform for the vibration signal collected from 5:30 on March 27.

results are insufficient to demonstrate that the incipient faults emerged on the planet gears at that time.

At 17:00 on March 28, severe faults have already arisen on the planet gears. The envelope spectrum of the reconstructed signal at different stages is shown in Fig. 12, where the fault characteristic frequency of planet gears (1.7 Hz) is clear but still weaker than the three times (0.93 Hz) of the rotating frequency of the rotor hub. The TQWT only using a low Q wavelet can detect planet gears fault as well. However, it is incapable of detecting incipient faults in Fig. 11. By contrast, the double Q wavelet-based sparse decomposition is effective in Figs 6b and 9.
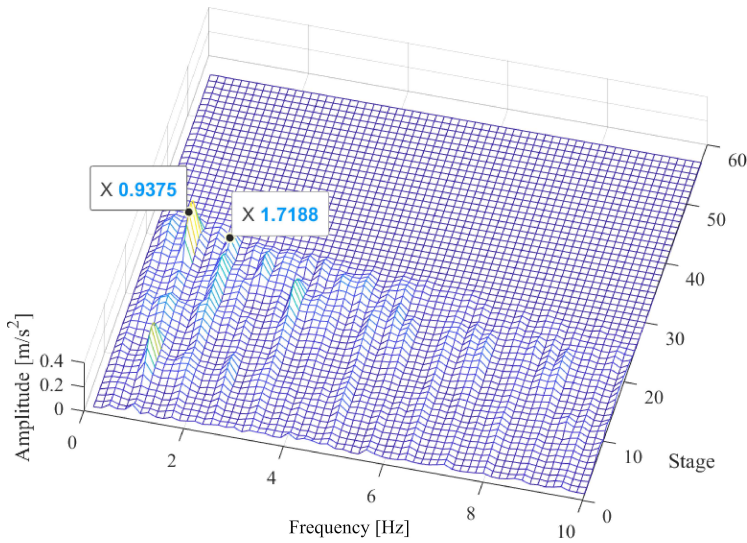

FIG. 12. The envelope spectrum of the reconstructed signal only using a low Q wavelet transform for the vibration signal collected from 17:00 on March 28.

Another classic fault analysis method – spectral kurtosis has been applied to compare the demodulation effect. The aim of spectral kurtosis is to find the most sensitive frequency band for faults through a series of bandpass filters. The kurtogram [20] is an effective tool that can realize the fast computation of the spectral kurtosis method. For the vibration signal collected from 5:30 on March 27, the kurtogram is shown in Fig. 13a. We filter the most sensitive frequency band (center frequency 60 Hz, bandwidth 40 Hz), and the envelope spectrum is shown in Fig. 13b. In this figure, the fault characteristic frequency of planet gears (1.72 Hz) exists but is submerged by the three times (0.96 Hz) of the rotating frequency of the rotor hub. Comparing to the decomposition result in Fig. 6b, it is hard to judge that planet gear was faulty at that time only through observing Fig. 13b.
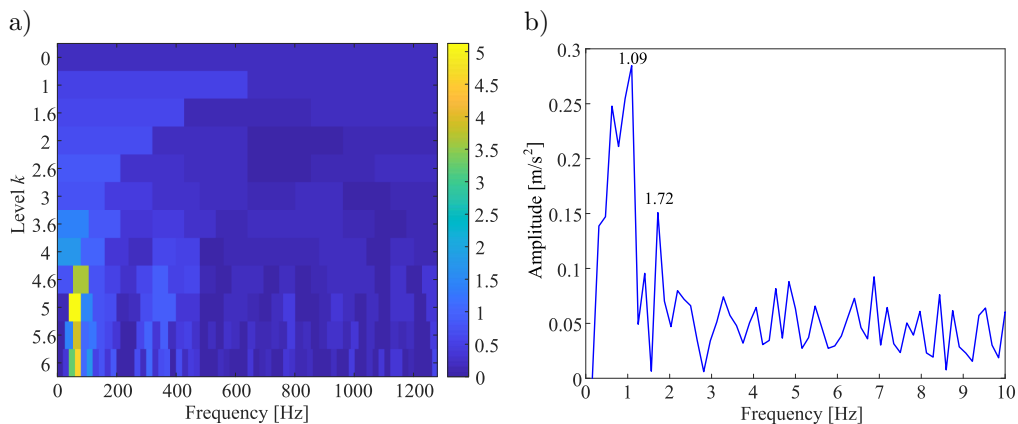
a)

b)

FIG. 13. The kurtogram of the vibration signal collected from 5:30 on March 27.

The kurtogram of the vibration signal collected from 17:00 on March 28 is shown in Fig. 14a. The center frequency of the sensitive frequency band is 240 Hz with a bandwidth of 53.33 Hz. The corresponding envelope spectrum is shown in Fig. 14b. In the figure, besides the three times (0.93 Hz) of the rotating frequency of the rotor hub and the fault characteristic frequency of planet gears (1.72 Hz), a series of harmonics with the interval 0.78 Hz are obvious. These intervals approximate half of the fault characteristic frequency of planet gears (0.86 Hz), indicating that the impacts from the ring gear and sun gear meshing with faulty planet gear are independent. The kurtogram has successfully extracted the fault characteristics of planet gears in the wind turbine gearbox, as shown in Fig. 14b. However, the demodulated energy is dispersed,
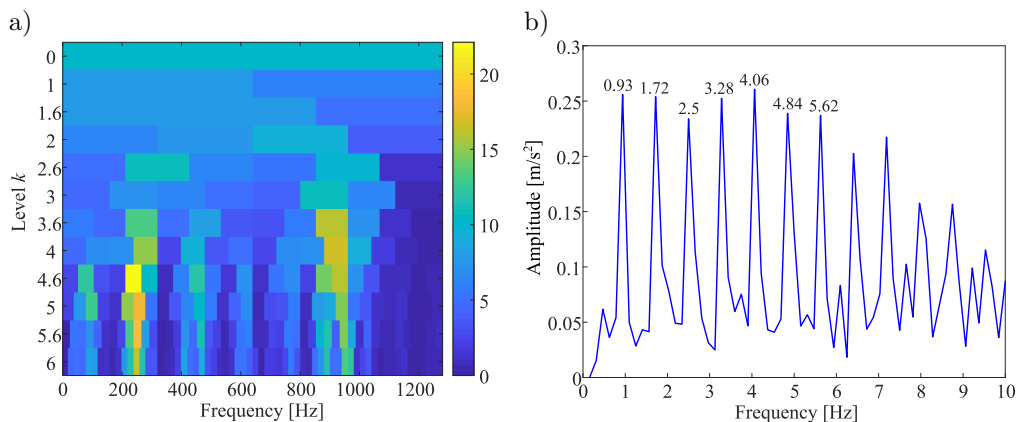
a)

b)

FIG. 14. The kurtogram of the vibration signal collected from 17:00 on March 28.

which is unfavorable to implementing automatic fault alarms by analyzing many harmonics. By contrast, the fault characteristic (red line with an arrow) in low Q components increases with the fault deterioration in Fig. 9 by the double Q wavelet-based sparse decomposition, exhibiting a superior tendency.

5. Conclusions

The structure of the wind turbine gearbox is complex, and the fault characteristics of the planetary stage gear set are usually concealed by the meshing vibration of higher-speed parallel gears and background noise. In this paper, the double Q wavelet sparse decomposition method was applied to extract fault features of the planetary gearbox of wind turbine. The complex vibration signals were decomposed into a high Q component dominated by gear meshing vibration and a low Q component dominated by fault impacts and background noise. Further, envelope demodulation of the low Q component clearly detected the weak fault features of the planet gear hidden in the complex background. The double Q wavelet-based sparse decomposition method can provide the technical guidance for the fault features extraction of planetary gears in wind turbine gearboxes.

References

1. http://www.xinhuanet.com/english/2021-07/12/c_1310057114.htm, accessed August 18, 2021.

2. https://gwec.net/global-wind-report-2021/ Global wind report 2021.

3. Feng Z., Zuo M.J., Vibration signal models for fault diagnosis of planetary gearboxes, *Journal of Sound and Vibration*, **331**(22): 4919–4939, 2012, doi: 10.1016/j.jsv.2012.05.039.

4. Feng Z., Chen X., Liang M., Iterative generalized synchrosqueezing transform for fault diagnosis of wind turbine planetary gearbox under nonstationary conditions, *Mechanical Systems and Signal Processing*, **52–53**: 360–375, 2015, doi: 10.1016/j.ymssp.2014.07.009.

5. Feng Z., Liang M., Fault diagnosis of wind turbine planetary gearbox under nonstationary conditions via adaptive optimal kernel time-frequency analysis, *Renewable Energy*, **66**: 468–477, 2014, doi: 10.1016/j.renene.2013.12.047.

6. Lei Y., Han D., Lin J., He Z., Planetary gearbox fault diagnosis using an adaptive stochastic resonance method, *Mechanical Systems and Signal Processing*, **38**(1): 113–124, 2013, doi: 10.1016/j.ymssp.2012.06.021.

7. Zhang J., Zhong M., Zhang J.Q., Yao L.G., Zheng J.D., An integrating methodology of Teager energy operator and stochastic resonance for incipient fault diagnosis of planetary gearbox [in Chinese], *Journal of Vibration Engineering*, **32**(6): 1084–1093, 2019.

8. Liang X., Zuo M. J., Hoseini M.R., Vibration signal modeling of a planetary gear set for tooth crack detection, *Engineering Failure Analysis*, **48**: 185–200, 2015, doi: 10.1016/j.engfailanal.2014.11.015.

9. SELESNICK I.W., Resonance-based signal decomposition: a new sparsity-enabled signal analysis method, *Signal Processing*, **91**(12): 2793–2809, 2011, doi: 10.1016/j.sigpro.2010.10.018.

10. SELESNICK I.W., Wavelet transform with tunable Q-factor, *IEEE Transactions on Signal Processing*, **59**(8): 3560–3575, 2011, doi: 10.1109/TSP.2011.2143711.

11. CAI G.G., CHEN X.F., HE Z.J., Sparsity-enabled signal decomposition using tunable Q-factor wavelet transform for fault feature extraction of gearbox, *Mechanical Systems and Signal Processing*, **41**(1–2): 34–53, 2013, doi: 10.1016/j.ymssp.2013.06.035.

12. DU Z., CHEN X., ZHANG H., YAN R., Sparse feature identification based on union of redundant dictionary for wind turbine gearbox fault diagnosis, *IEEE Transactions on Industrial Electronics*, **62**(10): 6594–6605, 2015, doi: 10.1109/TIE.2015.2464297.

13. HE W., CHEN B., ZENG N., ZI Y., Sparsity-based signal extraction using dual Q-factors for gearbox fault detection, *ISA Transactions*, **79**: 147–160, 2018, doi: 10.1016/j.isatra.2018.05.009.

14. TENG W., LIU Y., HUANG Y., SONG L., LIU Y., MA Z., Fault detection of planetary sub-assemblies in a wind turbine gearbox using TQWT based sparse representation, *Journal of Sound and Vibration*, **490**: 115707, 2021, doi: 10.1016/j.jsv.2020.115707.

15. SELESNICK I., Sparse regularization via convex analysis, *IEEE Transactions on Signal Processing*, **65**(17): 4481–4494, 2017, doi: 10.1109/TSP.2017.2711501.

16. CAI G., SELESNICK I.W., WANG S., DAI W., ZHU Z., Sparsity-enhanced signal decomposition via generalized minimax-concave penalty for gearbox fault diagnosis, *Journal of Sound and Vibration*, **432**: 213–234, 2018, doi: 10.1016/j.jsv.2018.06.037.

17. WANG L., CAI G., WANG .J, JIANG X., ZHU Z., Dual-enhanced sparse decomposition for wind turbine gearbox fault diagnosis, *IEEE Transactions on Instrumentation and Measurement*, **68**(2): 450–461, 2019, doi: 10.1109/TIM.2018.2851423.

18. DAUBECHIES I., *Ten Lectures on Wavelets*, Philadelphia, PA: SIAM, 1992.

19. FIGUEIREDO M.A.T., BIOUCAS-DIAS J.M., AFONSO M.V., Fast frame-based image deconvolution using variable splitting and constrained optimization, [in:] *2009 IEEE/SP 15th Workshop on Statistical Signal Processing*, pp. 109–112, 2009, doi: 10.1109/SSP.2009.5278628.

20. ANTONI J., Fast computation of the kurtogram for the detection of transient faults, *Mechanical Systems and Signal Processing*, **21**(1): 108–124, 2007, doi: 10.1016/j.ymssp.2005.12.002.